

Fluid flow through anisotropic and deformable double porosity media with ultra-low matrix permeability: A continuum framework

Qi Zhang^{a,*}, Xia Yan^b, Jianli Shao^c

^a*Department of Civil and Environmental Engineering, Stanford University, Stanford, CA 94305, USA*

^b*School of Petroleum Engineering, China University of Petroleum (East China), Qingdao, 266580, China*

^c*State Key Laboratory of Mining Disaster Prevention and Control, Shandong University of Science and Technology, Qingdao, 266590, China*

Abstract

Fractured porous media or double porosity media are common in nature. At the same time, accurate modeling remains a significant challenge due to bi-modal pore size distribution, anisotropy, multi-field coupling, and various flow patterns. This study aims to formulate a comprehensive coupled flow and solid deformation model of anisotropic and deformable double porosity media with ultra-low matrix permeability. Fluid in fissures is modeled with the generalized Darcy's law, while the liquid in much less permeable matrix follows a low-velocity non-Darcy flow characterized by threshold values and non-linearity, and fluid mass transfer is dependent on the shape factor, phase pressure difference, and interface permeability. The solid deformation relies on a thermodynamically consistent effective stress derived from the energy balance equation, and it is modeled following anisotropic poroelastic theory. Scaling analysis is performed to drop the negligible force density term under reasonable ranges of parameters. The discussion revolves around generic double porosity media. Numerical simulation of the initial boundary value problem reveals the capability of this framework to capture the crucial roles of coupling, anisotropy, and ultra-low matrix permeability in dictating the pressure and displacement fields.

Keywords: Double porosity, Geomechanics, Anisotropy, Ultra-low matrix permeability

1. Introduction

In our natural environment, the real reservoirs tend to be very heterogeneous in both porosity and permeability characteristics due to the existence of porous constituents at various length scales [1]. The accurate simulation of real reservoirs remains a significant challenge. Instead, people always idealize the actual reservoir as an aggregate of different geological regions (e.g., host rock, fracture, fault, compaction band, and so on), among which the fractured porous media is widely adopted in engineering practice. Sometimes fractured porous media is also called double (dual) porosity media. Although researchers in reservoir engineering firstly proposed the concept of fractured porous media [3, 30], nowadays, it has been widely used in other branches of earth sciences, with different terminologies to describe fracture and porous matrix. In the context of aggregated soils, they are usually termed macropores and micropores [10], whereas in the context for sedimentary rocks, we shall call them micro-cracks and nanopores [39]. It must be noted that

*Corresponding author

Email address: qzhang94@stanford.edu (Qi Zhang)

the macro-fractures which can be seen with the naked eye constitute another (much larger) porosity scale [40], which is not covered in the present discussion.

In fractured porous media, due to significant differences in the pore sizes, fluid transmission through the fissures and the rock matrix could be very distinctive. In most cases, fissures serve as the primary conduit for fluid flow, whereas the smaller pores in the rock matrix generally play a supporting role in the fluid transmission, and for the most part, simply discharge fluid into the fissures. Generally speaking, there are two classes of methods used for modeling fractured porous media: discrete (explicit) methods and continuum (implicit) methods [1]. Since dual continuum models can provide practical insight into the global behaviors of the multiscale system with much less computational cost [1], we focus on the continuum method while at the same time try to connect with the discrete descriptions of the fissures.

Darcy's law is the most fundamental equation to describe fluid flow in conventional reservoirs or micro-cracks. However, for unconventional and tight reservoirs with ultra-low matrix permeability (assuming isotropic), Darcy's law could overestimate the flow rate of liquid due to the interaction between fluid particles and the solid pore wall [13, 28, 34, 37]. The result of this interaction is the formation of a boundary layer on which the liquid exhibits higher viscosity [28]. In the literature, this phenomenon is known as low-velocity non-Darcy flow of liquid (lower limit of Darcy's law [13]) or nonlinear percolation [29]. It has been argued in the literature that when the magnitude of gradient is extremely small, say, lower than a scalar called threshold pressure gradient (TPG) [18], the boundary layer could prevent the fluid from flowing [24], and above this TPG, the flow curve in each direction shows a certain level of non-linearity [29], followed by a straight line [25]. In other words, Darcy's law should be corrected for the effect of the TPG. However, there also exist some opposite opinions about TPG [28], which asserted such threshold does not exist or it is a misinterpretation of experimental data, and they chose an alternative nonlinear model [28].

In addition to extensive investigations on flow problem, the tightly coupled hydromechanical behavior is central to the performance of many subsurface systems and is critical for assessing environmental impacts [6]. This strong coupling is always modeled as a two way coupled process, which is described by the well-established poromechanical theory for conventional single porosity media. For fractured porous media, a fair amount of papers have been published to consider solid deformation in both continuous and discrete senses. For continuum modeling, Wilson et al. [33] made the first attempt to consider solid deformation in double porosity media by introducing new governing equations as well as new material properties. Over the last 30 years, efforts along this line have resulted in seven main modeling approaches that are individually developed (for example, see [2, 4, 5, 7, 15, 20, 26]), and they differ in terms of assumptions and parameters. The representative authors for each modeling approach are (in alphabetical order of their last names): Abousleiman, Bai and Elsworth and Roegiers, Berryman and Wang, Borja, Chen, Khalili, Lewis. Almost all the discrepancies come from the actual modeling of porosity change and this remains, to the best of current authors' knowledge, an open question. For discrete modeling, Garipov et al. [14] combined DFM with fracture contact problem, leading to a fully implicit formulation of coupled flow and solid deformation for fractured three-dimensional subsurface formations. Jiang et al. [19] further considered the compaction and embedment of proppant in the fracture contact problem of a shale gas reservoir, and a splitting-node technique was used to deal with the discontinuities in the displacement field across the fracture interface. Yan et al. [35, 36] applied embedded discrete fracture matrix (EDFM) method to model macro-fractures and they also developed a stabilized extended finite element method (XFEM) to eliminate displacement oscillation along macro-fracture boundaries. We can see the difficulty for discrete modeling lies in the accurate characterizations of fracture behaviors and their impacts on flow and deformation.

This paper aims to develop a mathematically consistent framework for fluid flow through anisotropic and deformable double porosity media with ultra-low matrix permeability. All the derivations are presented

under the assumption of single phase flow and infinitesimal deformation. The paper is organized as follows: detailed mathematical formulations are first presented which adopt mixture poromechanics theory, but this time we reveal from the most general perspective which to the authors' knowledge, has never been proposed in the previous papers. Scaling analysis is performed to drop the negligible force density term, and a 3D numerical example is given in the end. In this paper, we use subscript 1 and 2 to represent primary porosity (porous blocks or micropores) and secondary porosity (fissures or macropores), respectively.

2. Fluid flow model

In continuum modeling of double porosity media, three mass conservation equations are built on the same overlapping domain, distinguished by Eulerian volume fractions $\phi_1 = V_1/V_b$, $\phi_2 = V_2/V_b$ and $1 - \phi_1 - \phi_2 = V_s/V_b$ where $V_b = V_1 + V_2 + V_s$ is the total (bulk) volume of the mixture. Following Eulerian description, above three mass conservation equations are given as [11]

$$\frac{\partial}{\partial t} [\rho_s (1 - \phi)] + \nabla \cdot [\rho_s (1 - \phi) \mathbf{v}_s] = 0, \quad (1)$$

$$\frac{\partial}{\partial t} [\rho_{1f} \phi_1] + \nabla \cdot [\rho_{1f} \phi_1 \hat{\mathbf{v}}_1] = c_1, \quad (2)$$

$$\frac{\partial}{\partial t} [\rho_{2f} \phi_2] + \nabla \cdot [\rho_{2f} \phi_2 \hat{\mathbf{v}}_2] = c_2, \quad (3)$$

where $\phi = \phi_1 + \phi_2$, ρ_s is the solid density, ρ_{1f} and ρ_{2f} are the fluid densities, \mathbf{v}_s is the velocity of the solid skeleton, $\hat{\mathbf{v}}_1$ and $\hat{\mathbf{v}}_2$ are the interstitial velocities or tracer velocities, c_1 and c_2 represent the source terms. If there is only mass exchange between domain 1 and domain 2, then $c_1 + c_2 = 0$.

The remaining task is to rewrite Eqs. (2)(3) into equivalent forms. To begin with, we need to introduce the material time derivative following a particular constituent (s or $1f$ or $2f$). The definitions are given here

$$\frac{d^s(\cdot)}{dt} = \frac{\partial(\cdot)}{\partial t} + \nabla(\cdot) \cdot \mathbf{v}_s, \quad (4)$$

$$\frac{d^{1f}(\cdot)}{dt} = \frac{\partial(\cdot)}{\partial t} + \nabla(\cdot) \cdot \hat{\mathbf{v}}_1, \quad (5)$$

$$\frac{d^{2f}(\cdot)}{dt} = \frac{\partial(\cdot)}{\partial t} + \nabla(\cdot) \cdot \hat{\mathbf{v}}_2. \quad (6)$$

In the following text, since we prefer material time derivative following the solid phase motion whenever possible, we could drop the superscript s in $d^s(\cdot)/dt$. For Eq. (2) and Eq. (3), the following processes are basically the same except for the change of the subscript. Thus we deal with Eq. (2) in detail and provide the final form of Eq. (3) at the end of my derivation. By expanding derivatives (time and space) in Eq. (2), we get

$$\rho_{1f} \frac{\partial \phi_1}{\partial t} + \phi_1 \frac{\partial \rho_{1f}}{\partial t} + \phi_1 \hat{\mathbf{v}}_1 \cdot \nabla \rho_{1f} + \rho_{1f} \nabla \cdot [\phi_1 \hat{\mathbf{v}}_1] = c_1. \quad (7)$$

In Eq. (7), after extraction of ϕ_1 , the combination of the second and the third terms on LHS is exactly the material time derivative of constituent $1f$. Adopting this definition and further dividing ρ_{1f} on both sides, we obtain

$$\frac{\partial \phi_1}{\partial t} + \frac{\phi_1}{\rho_{1f}} \frac{d^{1f} \rho_{1f}}{dt} + \nabla \cdot [\phi_1 \hat{\mathbf{v}}_1] = \frac{c_1}{\rho_{1f}}. \quad (8)$$

Now we need to define superficial velocity \mathbf{q}_1 in our context which is given as follows

$$\mathbf{q}_1 = \phi_1 (\hat{\mathbf{v}}_1 - \mathbf{v}_s) . \quad (9)$$

Then we can further rewrite Eq. (8) using \mathbf{q}_1 and we have

$$\frac{\partial \phi_1}{\partial t} + \frac{\phi_1}{\rho_{1f}} \frac{d^{1f} \rho_{1f}}{dt} + \nabla \cdot \mathbf{q}_1 + \nabla \cdot [\phi_1 \mathbf{v}_s] = \frac{c_1}{\rho_{1f}} . \quad (10)$$

We can further combine the first and last terms on LHS in Eq. (10), see below

$$\frac{\partial \phi_1}{\partial t} + \nabla \cdot [\phi_1 \mathbf{v}_s] = \frac{\partial \phi_1}{\partial t} + \mathbf{v}_s \cdot \nabla \phi_1 + \phi_1 \nabla \cdot \mathbf{v}_s = \frac{d\phi_1}{dt} + \phi_1 \nabla \cdot \mathbf{v}_s . \quad (11)$$

By substituting the result of Eq. (11) into Eq. (10), we would have

$$\frac{\phi_1}{\rho_{1f}} \frac{d^{1f} \rho_{1f}}{dt} + \nabla \cdot \mathbf{q}_1 + \frac{d\phi_1}{dt} + \phi_1 \nabla \cdot \mathbf{v}_s = \frac{c_1}{\rho_{1f}} . \quad (12)$$

Note in the literature it is possible to see alternative expressions of the first two terms in Eq. (12) [7]. In fact, we can prove following identical relation easily

$$\frac{\phi_1}{\rho_{1f}} \frac{d\rho_{1f}}{dt} + \frac{\nabla \cdot [\rho_{1f} \mathbf{q}_1]}{\rho_{1f}} = \frac{\phi_1}{\rho_{1f}} \frac{d^{1f} \rho_{1f}}{dt} + \nabla \cdot \mathbf{q}_1 . \quad (13)$$

For the detailed proof, see [Appendix A](#). If we further define the fluid bulk modulus K_{1f} (also known as the pressure-volume-temperature relationship), which can be expressed as

$$\frac{1}{\rho_{1f}} \frac{d^{1f} \rho_{1f}}{dt} = \frac{1}{K_{1f}} \frac{d^{1f} p_1}{dt}, \quad \frac{1}{\rho_{1f}} \frac{d\rho_{1f}}{dt} = \frac{1}{K_{1f}} \frac{dp_1}{dt}, \quad \frac{1}{\rho_{1f}} \frac{\partial \rho_{1f}}{\partial t} = \frac{1}{K_{1f}} \frac{\partial p_1}{\partial t}, \quad (14)$$

where p_1 is the fluid pressure. It is easy to verify following relation between ρ_{1f} and p_1 satisfies Eq. (14)

$$\rho_{1f} = \rho_f \exp\left(\frac{p_1 - p^0}{K_{1f}}\right), \quad (15)$$

where ρ_f is the reference fluid density and p^0 is the reference pressure. Equation (15) is used in this paper. Combining Eq. (14) and Eq. (12) gives

$$\frac{\phi_1}{K_{1f}} \frac{d^{1f} p_1}{dt} + \nabla \cdot \mathbf{q}_1 + \frac{d\phi_1}{dt} + \phi_1 \nabla \cdot \mathbf{v}_s = \frac{c_1}{\rho_{1f}} . \quad (16)$$

Exactly the same logic also applies to Eq. (3). As a result, we obtain

$$\frac{\phi_2}{K_{2f}} \frac{d^{2f} p_2}{dt} + \nabla \cdot \mathbf{q}_2 + \frac{d\phi_2}{dt} + \phi_2 \nabla \cdot \mathbf{v}_s = \frac{c_2}{\rho_{2f}} . \quad (17)$$

Until now, except for the assumption of the basic double porosity model which admits two overlapping continua and fluid compressibilities for $1f$ and $2f$, no additional assumption has been made in the preceding derivations to Eqs. (16)(17). In other words, we can regard Eqs. (16)(17) as the starting point to introduce all kinds of specific constitutive relations (approximations), among them the modeling of $d\phi_1/dt$ and $d\phi_2/dt$

is still an open question, and that is why we have at least seven different modeling approaches mentioned in Sec. 1. In this paper, we try to move one step further by proposing a new expression inspired by [1, 8, 9, 22] that could incorporate all the other existing modeling approaches. To motivate our expression, let us go back to the single porosity media. In single porosity media, we have

$$\delta\zeta \triangleq \frac{\delta V_p - \delta V_f}{V_b}, \quad (18)$$

where $\delta\zeta$ is the increment of fluid content, and above equation demonstrates that the increment of fluid content is the difference between the fractional change in pore volume and the fractional change in fluid volume [27]. The corresponding constitutive law for $\delta\zeta$ and δV_f are given as [9, 12, 27]

$$\delta\zeta = S_e \times \delta p + \alpha : \delta\epsilon, \quad (19)$$

$$\frac{\delta V_f}{V_b} = -\frac{\phi}{K_f} \delta p, \quad (20)$$

where S_e is the constrained specific storage (specific storage at constant strain [27]) and α is the Biot tensor. In addition, we have the following identical relation [7]

$$\frac{\delta V_p}{V_b} = \delta\phi + \phi \delta\epsilon_{\text{vol}}, \quad (21)$$

where ϵ_{vol} is the volumetric strain. Then we substitute Eqs. (19)(20)(21) into Eq. (18) and further divide both sides by δt and take limits $\delta t \rightarrow 0$, we come up with the following equation to model $d\phi/dt$

$$\frac{d\phi}{dt} = \underbrace{\left(S_e - \frac{\phi}{K_f} \right)}_{\text{Coupling coefficient}} \times \frac{dp}{dt} + (\alpha - \phi\mathbf{1}) : \frac{d\epsilon}{dt}. \quad (22)$$

A similar but isotropic version of Eq. (22) is derived in the Appendix B.5 of [22]. Motivated by Eq. (22) and given we now have two pressure fields and two porous regions (V_1 and V_2), we can propose the following abstract form to model $d\phi_1/dt$ and $d\phi_2/dt$ through a conceptual generalization which is consistent with the state equation Eq. (3.107) of “thermodynamics and the double porosity network” in [11]

$$\begin{Bmatrix} \frac{d\phi_1}{dt} \\ \frac{d\phi_2}{dt} \end{Bmatrix} = \begin{bmatrix} A_{11} & A_{12} \\ A_{21} & A_{22} \end{bmatrix} \begin{Bmatrix} \frac{dp_1}{dt} \\ \frac{dp_2}{dt} \end{Bmatrix} + \begin{Bmatrix} (\alpha_1 - \phi_1\mathbf{1}) : \frac{d\epsilon}{dt} \\ (\alpha_2 - \phi_2\mathbf{1}) : \frac{d\epsilon}{dt} \end{Bmatrix}, \quad (23)$$

where A is the generalized 2×2 coupling matrix instead of one single coupling coefficient, α_1 and α_2 are the symmetric Biot tensors, $\mathbf{1}$ is the second order identity tensor, $\epsilon = (\nabla\mathbf{u} + \mathbf{u}\nabla)/2$ is the infinitesimal strain tensor and \mathbf{u} is the solid displacement vector which satisfies $\mathbf{v}_s = \mathbf{d}\mathbf{u}/dt$. Equation (23) is used in Sec. 3 to manipulate linear momentum and energy balance equations.

Besides $d\phi_1/dt$ and $d\phi_2/dt$, we still need to provide expressions for \mathbf{q}_1 , \mathbf{q}_2 , c_1 and c_2 to close our mass balance formulation. For \mathbf{q}_1 , we assume it follows the low-velocity non-Darcy flow of liquid that can be expressed as a nonlinear function of $\varphi = \nabla p_1 - \rho_{1f}\mathbf{g}$

$$(\mathbf{q}_1)_j = \begin{cases} 0 & |\varphi_j| < \lambda_{\min}, \\ -\frac{k_1 (|\varphi_j| - \lambda_{\min})^\xi}{\mu_{1f} \xi \delta^{\xi-1}} \text{sgn}(\varphi_j) & \lambda_{\min} \leq |\varphi_j| \leq \lambda_{\max}, \\ -\frac{k_1}{\mu_{1f}} \left(|\varphi_j| - \lambda_{\min} - \frac{\xi-1}{\xi} \delta \right) \text{sgn}(\varphi_j) & |\varphi_j| > \lambda_{\max}, \end{cases} \quad (24)$$

where \mathbf{g} is the gravity acceleration vector, $j = 1, \dots, n_{\text{dim}}$ where n_{dim} is the space dimension, k_1 is the Darcy permeability of the matrix, μ_{1f} is the fluid viscosity, $\xi \geq 1$ is the exponent parameter [41], $\delta = \lambda_{\max} - \lambda_{\min}$, λ_{\min} has the physical meaning of threshold gradient and λ_{\max} has the physical meaning of critical gradient [41], the pseudo gradient of this model can be calculated analytically as $\lambda_{\min} + \delta(\xi - 1)/\xi$. In this paper, we assume ξ , λ_{\min} and λ_{\max} are constants. From Eq. (24), we can see that this non-Darcy flow model is a combination of a no flow part, a nonlinear flow part and a linear flow part, separated by λ_{\min} and λ_{\max} , which describes exactly the type curve of non-Darcy flow [42]. In addition, if we set $\xi = 1$ and $\lambda_{\min} = 0$, isotropic Darcy's law is automatically recovered. Thus Eq. (24) is more general than similar equations in [17, 25, 39]. For \mathbf{q}_2 , we assume it follows the generalized Darcy's law, which is given by the relation

$$\mathbf{q}_2 = -\frac{\mathbf{k}_2}{\mu_{2f}} \cdot (\nabla p_2 - \rho_{2f} \mathbf{g}). \quad (25)$$

Due to this full tensor permeability \mathbf{k}_2 , the direction of \mathbf{q}_2 depends on both pressure gradient and the principal directions of anisotropy [39]. Finally, for c_1 and c_2 , we adopt prototype in [30] with minor modifications

$$c_1 = \frac{\rho_f \sigma_{\text{sh}} \bar{k}}{\mu_f} (p_2 - p_1) + \text{MS}_1, \quad (26)$$

$$c_2 = \frac{\rho_f \sigma_{\text{sh}} \bar{k}}{\mu_f} (p_1 - p_2) + \text{MS}_2, \quad (27)$$

where σ_{sh} is the shape factor, \bar{k} is the interface permeability whose mathematical model is elaborated in the next paragraph, μ_f is the reference fluid viscosity, MS_1 and MS_2 represent other mechanisms besides mass transfer.

In double-porosity models, the interface permeability \bar{k} also depends on the apparent permeability $\partial \mathbf{q}_1 / \partial \boldsymbol{\varphi}$ of the matrix [21]. In other words, in double porosity media the term "non-Darcy flow" pertains not only to the flow through nearly impermeable matrix, but also to the discharge of fluid from the matrix into the fissures. Therefore, we propose following form for \bar{k} that is analogous to the variations of aquifer properties in space [16]

$$\bar{k} = \begin{cases} \bar{k}_{\min} & \varphi_{\max} < \lambda_{\min}, \\ \frac{\bar{k}_{\max} + \bar{k}_{\min}}{2} + \frac{\bar{k}_{\min} - \bar{k}_{\max}}{2} \cos \left[\pi \left(\frac{\varphi_{\max} - \lambda_{\min}}{\delta} \right)^{\xi} \right] & \lambda_{\min} \leq \varphi_{\max} \leq \lambda_{\max}, \\ \bar{k}_{\max} & \varphi_{\max} > \lambda_{\max}, \end{cases} \quad (28)$$

where \bar{k}_{\max} and \bar{k}_{\min} are the maximum and minimum interface permeabilities, respectively, and

$$\varphi_{\max} = \max_{j \in \{1, \dots, n_{\text{dim}}\}} |\varphi_j|. \quad (29)$$

When $\bar{k}_{\max} = \bar{k}_{\min}$, the interface permeability \bar{k} becomes a trivial constant, whereas when $\bar{k}_{\max} > \bar{k}_{\min}$ and as φ_{\max} decays, the decrease in \bar{k} due to the boundary layer effect is analogous to that which occurs when a small value of diffusion property is specified for clay layers or clay pods (immobile zone) [16]. Later we shall show that this variation in \bar{k} also affects the entire fluid flow patterns.

3. Solid deformation model

To address the issue of solid deformation, we need to define several “partial” quantities. First of all, we need to define partial stress tensor σ^a for every constituent $a = s, 1f$ and $2f$. By using Cauchy’s traction theorem, the σ^a is defined such that it linearly transforms a normal vector \mathbf{n} to a partial traction vector \mathbf{t}^a that equals the force δf_a acting on constituent a divided by the total area δA , i.e.,

$$\sigma^a \cdot \mathbf{n} = \mathbf{t}^a = \lim_{\delta A \rightarrow 0} \frac{\delta f_a}{\delta A}. \quad (30)$$

Secondly we need to define the partial density ρ^a as the mass of constituent a divided by the total volume, and we can relate ρ^a with ρ_a easily using porosity as

$$\rho^s = \rho_s (1 - \phi), \quad (31)$$

$$\rho^{1f} = \rho_{1f} \phi_1, \quad (32)$$

$$\rho^{2f} = \rho_{2f} \phi_2. \quad (33)$$

Thirdly, we use \mathbf{h}^a to represent the internal drag force on the constituent a by the surrounding other constituents divided by the total volume and it has the property that

$$\sum_a \mathbf{h}^a = \mathbf{0}. \quad (34)$$

Finally, $\hat{\mathbf{v}}_a$ represents the interstitial velocity for constituent a and it is just \mathbf{v}_s , $\hat{\mathbf{v}}_1$ and $\hat{\mathbf{v}}_2$ for constituents s , $1f$ and $2f$, respectively.

The balance of linear momentum for constituent a in integral form is given as follows

$$\int_A \sigma^a \cdot \mathbf{n} \, dA + \int_V \rho^a \mathbf{g} \, dV + \int_V \mathbf{h}^a \, dV = \frac{d^a}{dt} \int_V \rho^a \hat{\mathbf{v}}_a \, dV. \quad (35)$$

Note for the RHS of Eq. (35), we cannot interchange the time derivative and integral sign due to a moving control volume V . As a result, we need to use Reynold transport theorem to simplify RHS as

$$\frac{d^a}{dt} \int_V \rho^a \hat{\mathbf{v}}_a \, dV = \int_V \left[\frac{\partial \rho^a}{\partial t} + \nabla \cdot (\rho^a \hat{\mathbf{v}}_a) \right] \hat{\mathbf{v}}_a \, dV + \int_V \rho^a \mathbf{a}_a \, dV, \quad (36)$$

where $\mathbf{a}_a = d^a \hat{\mathbf{v}}_a / dt$. Surprisingly, the term inside the square bracket is exactly the LHS of Eqs. (1)(2)(3). Therefore, we can further simplify Eq. (36) as

$$\frac{d^a}{dt} \int_V \rho^a \hat{\mathbf{v}}_a \, dV = \int_V c_a \hat{\mathbf{v}}_a \, dV + \int_V \rho^a \mathbf{a}_a \, dV, \quad (37)$$

where we assume $c_s = 0$, $c_{1f} = c_1$ and $c_{2f} = c_2$. For LHS of Eq. (35), we just use divergence theorem and we obtain

$$\int_V [\nabla \cdot \sigma^a + \rho^a \mathbf{g} + \mathbf{h}^a] = \int_V c_a \hat{\mathbf{v}}_a \, dV + \int_V \rho^a \mathbf{a}_a \, dV. \quad (38)$$

Now we can apply the localization theorem to drop the integral sign and get partial differential equation as

$$\nabla \cdot \sigma^a + \rho^a \mathbf{g} + \mathbf{h}^a = c_a \hat{\mathbf{v}}_a + \rho^a \mathbf{a}_a. \quad (39)$$

The deformation equations for the entire mixture under quasi-static condition is obtained by summing Eq. (39) for all constituents, using Eq. (34) and setting $\mathbf{a}_a = \mathbf{0}$, this yields

$$\nabla \cdot \boldsymbol{\sigma} + \rho \mathbf{g} = \bar{\mathbf{c}}, \quad (40)$$

where $\boldsymbol{\sigma} = \sum_a \boldsymbol{\sigma}^a$ is the total Cauchy stress tensor, $\rho = \sum_a \rho^a$ is the bulk density, $\bar{\mathbf{c}} = c_1 \hat{\mathbf{v}}_1 + c_2 \hat{\mathbf{v}}_2$ is the additional momentum supply exerted by c_1 and c_2 .

Constitutive theory for granular materials is usually expressed in terms of the effective stress [38], so defining its mathematical form as a function of the total stress and fluid pressures is crucial for constitutive modeling. The expression for effective stress can be established with the aid of the first law of thermodynamics. To proceed, we denote by e the internal energy per unit total mass of the mixture. Without loss of generality we shall assume an isothermal process, i.e., we consider only mechanical terms. Next we define another variable \mathcal{E} such that it satisfies

$$\frac{dI}{dt} = \frac{d}{dt} \int_V \rho e \, dV = \int_V \frac{d\mathcal{E}}{dt} \, dV. \quad (41)$$

The first law of thermodynamics says

$$\int_V \frac{d\mathcal{E}}{dt} \, dV = P^{ME} - \sum_a \frac{d^a}{dt} \int_V \frac{\rho^a \hat{\mathbf{v}}_a \cdot \hat{\mathbf{v}}_a}{2} \, dV. \quad (42)$$

If we follow the same logic as shown in Eqs. (36)(37), we can rewrite above equation as

$$\int_V \frac{d\mathcal{E}}{dt} \, dV = P^{ME} - \sum_a \int_V \frac{c_a \hat{\mathbf{v}}_a \cdot \hat{\mathbf{v}}_a}{2} \, dV - \sum_a \int_V \rho^a \hat{\mathbf{v}}_a \cdot \mathbf{a}_a \, dV. \quad (43)$$

The mechanical power P^{ME} is the sum of the powers of \mathbf{t}^a , $\rho^a \mathbf{g}$ and \mathbf{h}^a for all constituents, which is shown here

$$P^{ME} = \sum_a \left[\int_A (\boldsymbol{\sigma}^a \cdot \mathbf{n}) \cdot \hat{\mathbf{v}}_a \, dA + \int_V \rho^a \mathbf{g} \cdot \hat{\mathbf{v}}_a \, dV + \int_V \mathbf{h}^a \cdot \hat{\mathbf{v}}_a \, dV \right] \quad (44)$$

Applying divergence theorem on the first term of RHS yields

$$\int_A (\boldsymbol{\sigma}^a \cdot \mathbf{n}) \cdot \hat{\mathbf{v}}_a \, dA = \int_V (\nabla \cdot \boldsymbol{\sigma}^a) \cdot \hat{\mathbf{v}}_a \, dV + \int_V \boldsymbol{\sigma}^a : \mathbf{l}_a \, dV, \quad (45)$$

where $\mathbf{l}_a = (\nabla \hat{\mathbf{v}}_a + \hat{\mathbf{v}}_a \nabla) / 2$ is the infinitesimal strain rate tensor of constituent a . Thus, we can rewrite Eq. (44) as

$$P^{ME} = \sum_a \left[\int_V (\nabla \cdot \boldsymbol{\sigma}^a) \cdot \hat{\mathbf{v}}_a \, dV + \int_V \boldsymbol{\sigma}^a : \mathbf{l}_a \, dV + \int_V \rho^a \mathbf{g} \cdot \hat{\mathbf{v}}_a \, dV + \int_V \mathbf{h}^a \cdot \hat{\mathbf{v}}_a \, dV \right]. \quad (46)$$

Combing Eqs. (43)(46) yields

$$\int_V \frac{d\mathcal{E}}{dt} \, dV = \sum_a \left[\int_V (\nabla \cdot \boldsymbol{\sigma}^a + \rho^a \mathbf{g} + \mathbf{h}^a - \rho^a \mathbf{a}_a) \cdot \hat{\mathbf{v}}_a \, dV + \int_V \boldsymbol{\sigma}^a : \mathbf{l}_a \, dV - \int_V \frac{c_a \hat{\mathbf{v}}_a \cdot \hat{\mathbf{v}}_a}{2} \, dV \right]. \quad (47)$$

Now we need to use balance of linear momentum Eq. (39) to replace $\nabla \cdot \boldsymbol{\sigma}^a + \rho^a \mathbf{g} + \mathbf{h}^a - \rho^a \mathbf{a}_a$, the result is

$$\int_V \frac{d\mathcal{E}}{dt} \, dV = \sum_a \left[\int_V \frac{c_a \hat{\mathbf{v}}_a \cdot \hat{\mathbf{v}}_a}{2} \, dV + \int_V \boldsymbol{\sigma}^a : \mathbf{l}_a \, dV \right]. \quad (48)$$

Again, if we apply localization theorem to above equation, we reach our first milestone

$$\frac{d\mathcal{E}}{dt} = \frac{1}{2} \sum_a c_a \hat{\mathbf{v}}_a \cdot \hat{\mathbf{v}}_a + \sum_a \boldsymbol{\sigma}^a : \mathbf{l}_a. \quad (49)$$

However, there are still something else that we can do with $\sum_a \boldsymbol{\sigma}^a : \mathbf{l}_a$ in Eq. (49). Let us expand it

$$\sum_a \boldsymbol{\sigma}^a : \mathbf{l}_a = \boldsymbol{\sigma}^s : \mathbf{l}_s + \boldsymbol{\sigma}^{1f} : \mathbf{l}_{1f} + \boldsymbol{\sigma}^{2f} : \mathbf{l}_{2f}. \quad (50)$$

In the following text we use \mathbf{l} to represent \mathbf{l}_s since this is the quantity that we are interested in. From the definition of total Cauchy stress tensor $\boldsymbol{\sigma}$, we know $\boldsymbol{\sigma}^s = \boldsymbol{\sigma} - \boldsymbol{\sigma}^{1f} - \boldsymbol{\sigma}^{2f}$ and if we substitute this relation into Eq. (50), we get

$$\sum_a \boldsymbol{\sigma}^a : \mathbf{l}_a = \boldsymbol{\sigma} : \mathbf{l} + \boldsymbol{\sigma}^{1f} : (\mathbf{l}_{1f} - \mathbf{l}) + \boldsymbol{\sigma}^{2f} : (\mathbf{l}_{2f} - \mathbf{l}). \quad (51)$$

Now we assume $\boldsymbol{\sigma}^{1f}$ and $\boldsymbol{\sigma}^{2f}$ are isotropic and can be represented as $\boldsymbol{\sigma}^{1f} = -\phi_1 p_1 \mathbf{1}$ and $\boldsymbol{\sigma}^{2f} = -\phi_2 p_2 \mathbf{1}$. From the definition of \mathbf{l}_a , we can easily prove $\mathbf{1} : (\mathbf{l}_{1f} - \mathbf{l}) = \nabla \cdot (\hat{\mathbf{v}}_1 - \mathbf{v}_s)$ and $\mathbf{1} : (\mathbf{l}_{2f} - \mathbf{l}) = \nabla \cdot (\hat{\mathbf{v}}_2 - \mathbf{v}_s)$. Therefore,

$$\sum_a \boldsymbol{\sigma}^a : \mathbf{l}_a = \boldsymbol{\sigma} : \mathbf{l} - \phi_1 p_1 \nabla \cdot (\hat{\mathbf{v}}_1 - \mathbf{v}_s) - \phi_2 p_2 \nabla \cdot (\hat{\mathbf{v}}_2 - \mathbf{v}_s). \quad (52)$$

From the definition of \mathbf{q}_1 and \mathbf{q}_2 , we know

$$\nabla \cdot \mathbf{q}_1 = \nabla \cdot [\phi_1 (\hat{\mathbf{v}}_1 - \mathbf{v}_s)] \simeq \phi_1 \nabla \cdot (\hat{\mathbf{v}}_1 - \mathbf{v}_s) \quad (53)$$

and

$$\nabla \cdot \mathbf{q}_2 = \nabla \cdot [\phi_2 (\hat{\mathbf{v}}_2 - \mathbf{v}_s)] \simeq \phi_2 \nabla \cdot (\hat{\mathbf{v}}_2 - \mathbf{v}_s) \quad (54)$$

given $(\hat{\mathbf{v}}_1 - \mathbf{v}_s) \cdot \nabla \phi_1$ and $(\hat{\mathbf{v}}_2 - \mathbf{v}_s) \cdot \nabla \phi_2$ are relatively small. At the same time, $\nabla \cdot \mathbf{q}_1$ and $\nabla \cdot \mathbf{q}_2$ also appear in Eqs. (16)(17), respectively. As a result, we can represent $\phi_1 p_1 \nabla \cdot (\hat{\mathbf{v}}_1 - \mathbf{v}_s)$ and $\phi_2 p_2 \nabla \cdot (\hat{\mathbf{v}}_2 - \mathbf{v}_s)$ in Eq. (52) in terms of other items using Eqs. (16)(17)(53)(54)

$$\phi_1 p_1 \nabla \cdot (\hat{\mathbf{v}}_1 - \mathbf{v}_s) = p_1 \nabla \cdot \mathbf{q}_1 = p_1 \left[\frac{c_1}{\rho_{1f}} - \frac{\phi_1}{K_{1f}} \frac{d^{1f} p_1}{dt} - \frac{d\phi_1}{dt} - \phi_1 \nabla \cdot \mathbf{v}_s \right], \quad (55)$$

$$\phi_2 p_2 \nabla \cdot (\hat{\mathbf{v}}_2 - \mathbf{v}_s) = p_2 \nabla \cdot \mathbf{q}_2 = p_2 \left[\frac{c_2}{\rho_{2f}} - \frac{\phi_2}{K_{2f}} \frac{d^{2f} p_2}{dt} - \frac{d\phi_2}{dt} - \phi_2 \nabla \cdot \mathbf{v}_s \right]. \quad (56)$$

Then we can insert Eqs. (55)(56) into Eq. (52) and further substitute the new Eq. (52) and abstract form Eq. (23) into Eq. (49), we reach our second milestone

$$\begin{aligned} \frac{d\mathcal{E}}{dt} = & \boldsymbol{\sigma} : \mathbf{l} + \frac{c_1 \hat{\mathbf{v}}_1 \cdot \hat{\mathbf{v}}_1}{2} + \frac{c_2 \hat{\mathbf{v}}_2 \cdot \hat{\mathbf{v}}_2}{2} \\ & + p_1 \left[\frac{\phi_1}{K_{1f}} \frac{d^{1f} p_1}{dt} + A_{11} \frac{dp_1}{dt} + A_{12} \frac{dp_2}{dt} + \boldsymbol{\alpha}_1 : \frac{d\boldsymbol{\epsilon}}{dt} - \frac{c_1}{\rho_{1f}} \right] \\ & + p_2 \left[\frac{\phi_2}{K_{2f}} \frac{d^{2f} p_2}{dt} + A_{21} \frac{dp_1}{dt} + A_{22} \frac{dp_2}{dt} + \boldsymbol{\alpha}_2 : \frac{d\boldsymbol{\epsilon}}{dt} - \frac{c_2}{\rho_{2f}} \right]. \end{aligned} \quad (57)$$

Now we just need to use the definition $\mathbf{l} = d\boldsymbol{\epsilon}/dt$ and we can rewrite above Eq. (57) into an equivalent form

$$\begin{aligned} \frac{d\mathcal{E}}{dt} &= (\boldsymbol{\sigma} + \alpha_1 p_1 + \alpha_2 p_2) : \mathbf{l} + \frac{c_1 \hat{\mathbf{v}}_1 \cdot \hat{\mathbf{v}}_1}{2} + \frac{c_2 \hat{\mathbf{v}}_2 \cdot \hat{\mathbf{v}}_2}{2} \\ &+ p_1 \left[\frac{\phi_1}{K_{1f}} \frac{d^{1f} p_1}{dt} + A_{11} \frac{dp_1}{dt} + A_{12} \frac{dp_2}{dt} - \frac{c_1}{\rho_{1f}} \right] \\ &+ p_2 \left[\frac{\phi_2}{K_{2f}} \frac{d^{2f} p_2}{dt} + A_{21} \frac{dp_1}{dt} + A_{22} \frac{dp_2}{dt} - \frac{c_2}{\rho_{2f}} \right]. \end{aligned} \quad (58)$$

This is our final destination. In this Eq. (58)

$$\bar{\boldsymbol{\sigma}} = \boldsymbol{\sigma} + \alpha_1 p_1 + \alpha_2 p_2 \quad (59)$$

is identified as the effective Cauchy stress tensor. Here we assume vertically transversely isotropic (VTI) linear elasticity, which is given by the constitutive relation in the Voigt notation

$$\begin{Bmatrix} \boldsymbol{\epsilon}_x \\ \boldsymbol{\epsilon}_y \\ \boldsymbol{\epsilon}_z \\ 2\boldsymbol{\epsilon}_{xy} \\ 2\boldsymbol{\epsilon}_{xz} \\ 2\boldsymbol{\epsilon}_{yz} \end{Bmatrix} = \underbrace{\begin{bmatrix} \frac{1}{E_h} & -\frac{\nu_{hh}}{E_h} & -\frac{\nu_{vh}}{E_v} \\ -\frac{\nu_{hh}}{E_h} & \frac{1}{E_h} & -\frac{\nu_{vh}}{E_v} \\ -\frac{\nu_{hv}}{E_h} & -\frac{\nu_{hv}}{E_h} & \frac{1}{E_v} \\ 0 & 0 & \frac{2(1+\nu_{hh})}{E_h} \\ 0 & \frac{1}{G_{vh}} & 0 \\ 0 & 0 & \frac{1}{G_{vh}} \end{bmatrix}}_S \begin{Bmatrix} \bar{\sigma}_x \\ \bar{\sigma}_y \\ \bar{\sigma}_z \\ \bar{\sigma}_{xy} \\ \bar{\sigma}_{xz} \\ \bar{\sigma}_{yz} \end{Bmatrix}. \quad (60)$$

From displacement reciprocal theorem, we have

$$\frac{\nu_{vh}}{E_v} = \frac{\nu_{hv}}{E_h}, \quad (61)$$

which guarantees the symmetry of the compliant matrix S . The elastic Poisson's ratio ν_{vh} should be understood as the stress applied in the vertical (bed-normal BN) direction and strain measured in the horizontal (bed-parallel BP) direction, ν_{hv} should be interpreted as the stress applied in the horizontal (bed-parallel BP) direction and strain measured in the vertical (bed-normal BN) direction, G_{vh} is the shear modulus along the BN direction, E_h and E_v are two Young's moduli. Note all the elastic constants are drained quantities. If $E_h = E_v = E$, $\nu_{vh} = \nu_{hv} = \nu$ and $G_{vh} = G = 0.5E/(1+\nu)$, then we restore the isotropic linear elasticity. Note both VTI linear elasticity and isotropic linear elasticity are just special cases of the anisotropic linear elasticity.

4. Flowchart

The flowchart of mathematical formulations of the previous two sections is shown in Fig. 1.

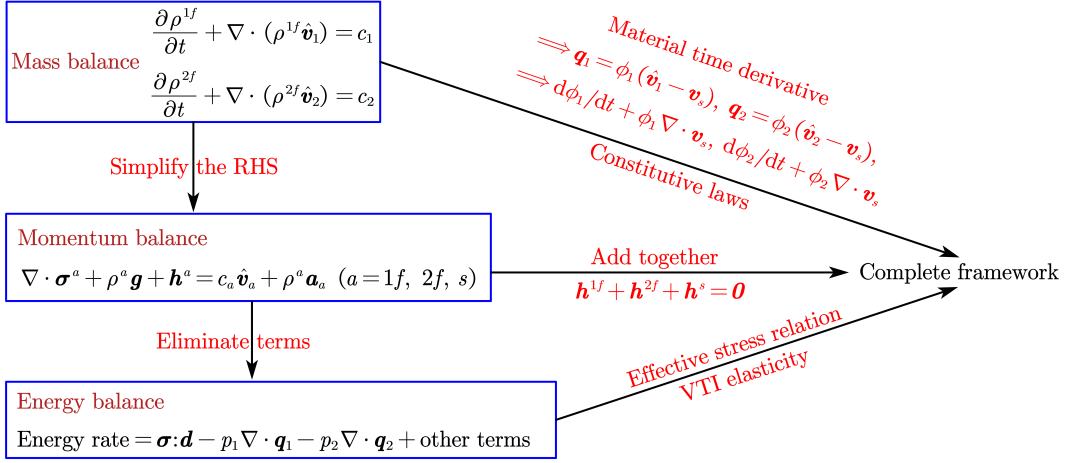


Figure 1: The interactions and relationships among different components of mathematical theories, and the way to obtain a complete framework.

5. Scaling analysis

In Eq. (40), there is no direct constitutive formula to calculate \bar{c} . However, we could show through scaling analysis, we can drop this term safely. First of all, we need to define some characteristic quantities. For ∇p_2 and $p_1 - p_2$, we assume $\mathcal{O}(\nabla p_2) = \Delta P/L$ and $\mathcal{O}(p_1 - p_2) = \Delta P_d$ where ΔP and ΔP_d represent the characteristic pressure variations, L is the characteristic length. Thus $\mathcal{O}(\nabla p_1) = \Delta P/L + \Delta P_d/L$. For α_1 , α_2 and porosities, we have $\mathcal{O}(\alpha_1) = \mathcal{O}(\alpha_2) = \mathcal{O}(\phi_1) = \mathcal{O}(\phi_2) = 1$, therefore, the force density term $\nabla \cdot (\alpha_1 p_1 + \alpha_2 p_2)$ has the order of $2\Delta P/L + \Delta P_d/L$. For $\hat{v}_1 - v_s$ and $\hat{v}_2 - v_s$, we quantify them using Darcy's law, as a result, $\mathcal{O}(\hat{v}_1 - v_s) = k_1 (\Delta P + \Delta P_d) / (\mu_f L)$ and $\mathcal{O}(\hat{v}_2 - v_s) = k_2 \Delta P / (\mu_f L)$ where k_1 , k_2 and μ_f are the characteristic quantities. Finally, for c_1 and c_2 , we can use Eqs. (26)(27) to get $\mathcal{O}(c_1) = \mathcal{O}(c_2) = \rho_f \sigma_{sh} k_1 \Delta P_d / \mu_f$ where ρ_f and σ_{sh} are also the characteristic quantities and we further adopt $\mathcal{O}(\bar{k}) = k_1$.

To argue that we can drop \bar{c} in Eq. (40) safely, we calculate the following dimensionless quantity

$$N_D = \frac{\mathcal{O}(c_1 \hat{v}_1 + c_2 \hat{v}_2)}{\mathcal{O}(\nabla \cdot (\alpha_1 p_1 + \alpha_2 p_2))} = \frac{\mathcal{O}(c_1 (\hat{v}_1 - v_s) + c_2 (\hat{v}_2 - v_s))}{\mathcal{O}(\nabla \cdot (\alpha_1 p_1 + \alpha_2 p_2))}. \quad (62)$$

Here we adopt following values: $k_1 = 10^{-15} \text{ m}^2$, $k_2 = 10^{-10} \text{ m}^2$, $\sigma_{sh} = 1000 \text{ m}^{-2}$, $\mu_f = 1 \text{ cP}$ and $\rho_f = 1000 \text{ kg/m}^3$. We plot N_D as a function of ΔP and ΔP_d , both under the same reasonable range from 1 kPa to 1 GPa (Reynolds number cannot be infinite). The result is shown in Fig. 2 which supports our argument and similar assertion can also be found in [1, 23].

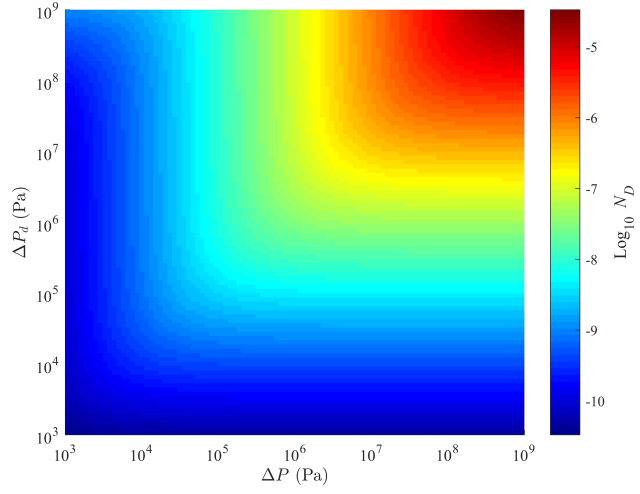


Figure 2: Scaling analysis result: Quantify \bar{c} vs. $\nabla \cdot (\alpha_1 p_1 + \alpha_2 p_2)$.

6. Numerical example

In this paper, we use the “ \mathbf{u} (quadratic) / p_1 (linear) / p_2 (linear)” finite element (FE) formulation that satisfies inf-sup condition [10, 31] to solve the problem numerically. Although this discretization scheme cannot guarantee element-wise mass conservation compared with finite volume (FV) formulation, it satisfies dual-grid mass conservation and it is still applicable to a homogeneous system or the system with mild heterogeneity to benefit from more desirable accuracy. Besides, the finite element method deals with the full tensor permeability very efficiently, which has an advantage over messy expressions in multi-point flux approximation (MPFA). The derivations of residual vectors $\mathcal{R}(X)$ and tangent operators $d\mathcal{R}/dX$ are similar to those in [10, 39] except for the explicit treatment of \bar{k} due to the sharp edge (non-differentiability) in the surface of φ_{\max} as a function of φ (see Fig. 3 for the illustration), i.e., $\bar{k} = \bar{k}^{t_n}$ is calculated from $\varphi^{t_n} = \nabla p_1^{t_n} - \rho_f \mathbf{g}$.

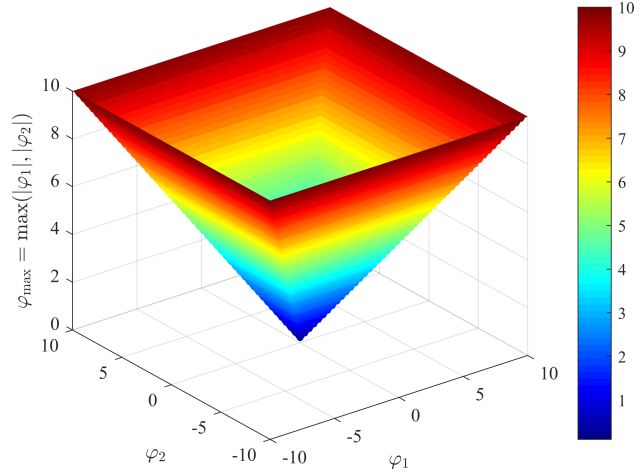


Figure 3: A simple illustration of the sharp edge in the surface of φ_{\max} as a function of $\varphi = (\varphi_1, \varphi_2)$ in 2D.

For code verification, we use the third example in [6] which is strip load on the infinite half space truncated at L . Here, we slightly modify the original drainage boundary condition Eqs. (A.7e)(A.7f) in [6] to be $p = 0$ on $\Gamma_{t2} \times I$ and $-\mathbf{q} \cdot \mathbf{n} = 0$ on $(\Gamma_{t1} \cup \Gamma_l \cup \Gamma_b \cup \Gamma_r) \times I$, respectively. The parameters are shown in Table 1 ^A and we compare result of our model with that of ANSYS, see Fig. 4. Note in Fig. 4, the dimensionless time T is defined as

$$T = \frac{E(1-\nu)kt}{(1+\nu)(1-2\nu)\mu_f a^2}. \quad (63)$$

Table 1: Parameter table of the verification example (with gravity).

Parameter	Value	Unit
Gravity acceleration constant g	9.81	m/s^2
Model size L	5 [6]	m
Half strip load length a	1 [6]	m
External mechanical load w	150 [6]	kPa
Unjacketed bulk modulus K_s	$+\infty$	kPa
Solid grain density ρ_s	2600	kg/m^3
Young's modulus E	6300	kPa
Poisson's ratio ν	0.15	-
Porosity ϕ_1	0.1	-
Porosity ϕ_2	0	-
Permeability $k_1 = k$	10^{-10}	m^2
Viscosity μ_f	1	cP
Fluid bulk modulus K_f	$+\infty$	kPa
Fluid density ρ_f	1000	kg/m^3

^AIsotropic elasticity. Darcy's law is applied to calculate $\mathbf{q}_1 = \mathbf{q}$ and since $\phi_2 = 0$, \mathbf{k}_2 , \bar{k} and σ_{sh} are not used.

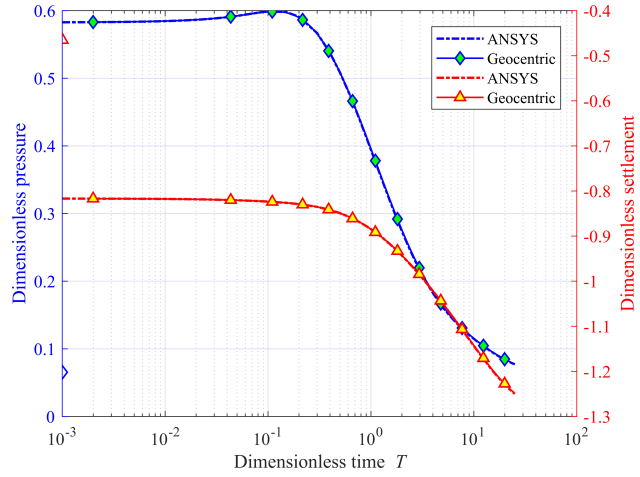


Figure 4: Result comparison of ANSYS and Geocentric. We choose to plot dimensionless pressure p/w and dimensionless settlement $Gu_y/w/a$ vs. T at 1 m below the center of the strip load. The two isolated points on the left represent initial values after normal consolidation which imply instantaneous changes in the pressure and displacement fields [6]. A perfect match is achieved here.

A 3D synthetic model is generated to contain superimposed porosity domains and horizontal planes of isotropy for both \mathbf{S} and \mathbf{k}_2 . The configuration of the problem and boundary (loading) conditions are shown in Fig. 5. This model could be recast into the famous Cryer's problem in the limit of single porosity and isotropy [10, 32]. The parameters are summarized in Table 2 and we have meshed this 3D synthetic model into 3456 hexahedron elements. The simulation begins with a time increment of 0.05 s and with subsequent increments magnified by a factor of 1.125, i.e., $\Delta t_{n+1} = 1.125\Delta t_n$. The total number of simulation time steps is 75.

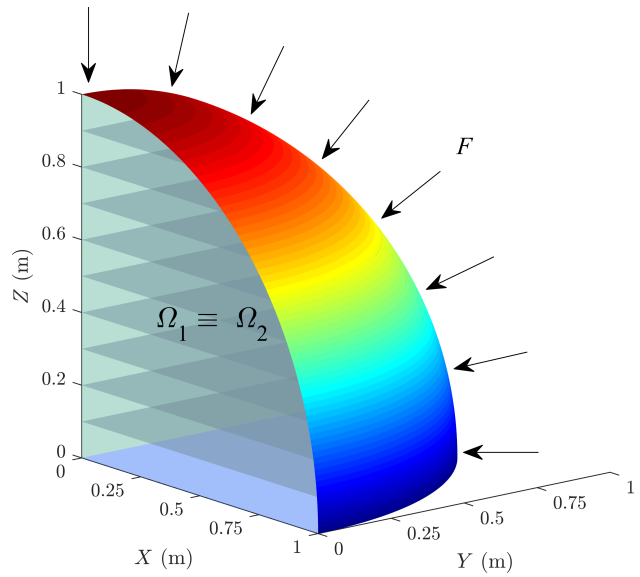


Figure 5: 3D compression problem of the 1/8 saturated poroelastic double porosity sphere. The gray horizontal planes indicate a VTI medium. Radial load F is applied on the spherical surface with rainbow color, which also serves as a drainage boundary but only for fissures. The other three surfaces that coincide with coordinate planes are impermeable with zero normal displacements. Gravity is not included in the analysis for this problem, i.e., excess form.

Table 2: Parameter table of the synthetic model (no gravity).

Parameter	Value	Unit
Time t	0.05 to 2744.3271	s
External mechanical load F	$1 + 0.5 \cos X$	MPa
Young's modulus E_v	5000	kPa
Young's modulus E_h	7500	kPa
Poisson's ratio ν_{vh}	0.25	-
Poisson's ratio ν_{hh}	0.15	-
Shear modulus G_{vh}	3000	kPa
Biot tensor α_1	$0.8 \times \mathbf{1}$	-
Biot tensor α_2	$0.2 \times \mathbf{1}$	-
Matrix A	[0.0358, -0.0358; -0.0358, 0.0358]	1/MPa
Permeability k_1	10^{-15} [42]	m^2
Critical gradient λ_{\max}	0.2306 [18, 41]	MPa/m
Threshold gradient λ_{\min}	0 [25]	MPa/m
Exponent parameter ξ	2 [25, 41]	-
Equivalent permeability k_{2H}	2.5×10^{-13}	m^2
Equivalent permeability k_{2V}	$0.02k_{2H}$	m^2
Maximum interface permeability \bar{k}_{\max}	10^{-15}	m^2
Minimum interface permeability \bar{k}_{\min}	$0.75\bar{k}_{\max}$	m^2
Shape factor σ_{sh}	2000	m^{-2}
Viscosity μ_f	1	cP
Fluid bulk modulus K_f	$+\infty$	kPa

The evolutions of p_1 and p_2 on the deformed domain are depicted in Fig. 6. For the first column, we can see that the early time response of p_1 is dependent on the spatial distribution of F since it is the fluid in the primary porosity that supports a large portion of the load in the beginning. Note here in mixture poromechanics theory, the secondary porosity is all void space, which means the underlying fracture has no intrinsic stiffness, so we cannot think of excess pressure accumulation in terms of the relative magnitude of intrinsic stiffness. For the second column, we can see that a permeability tensor with a high anisotropy ratio may not skew the pressure distribution. This is because in our case, the plane of isotropy intersects with the drainage boundary, which leads to a horizontal preferential fluid flow direction and as a result, the magnitude of k_{2V} doesn't control the pattern of p_2 . Furthermore, by comparing these two columns, we may conclude that in this case, non-equilibrium flow appears as soon as when we apply the load F , and it becomes weaker at a later stage.

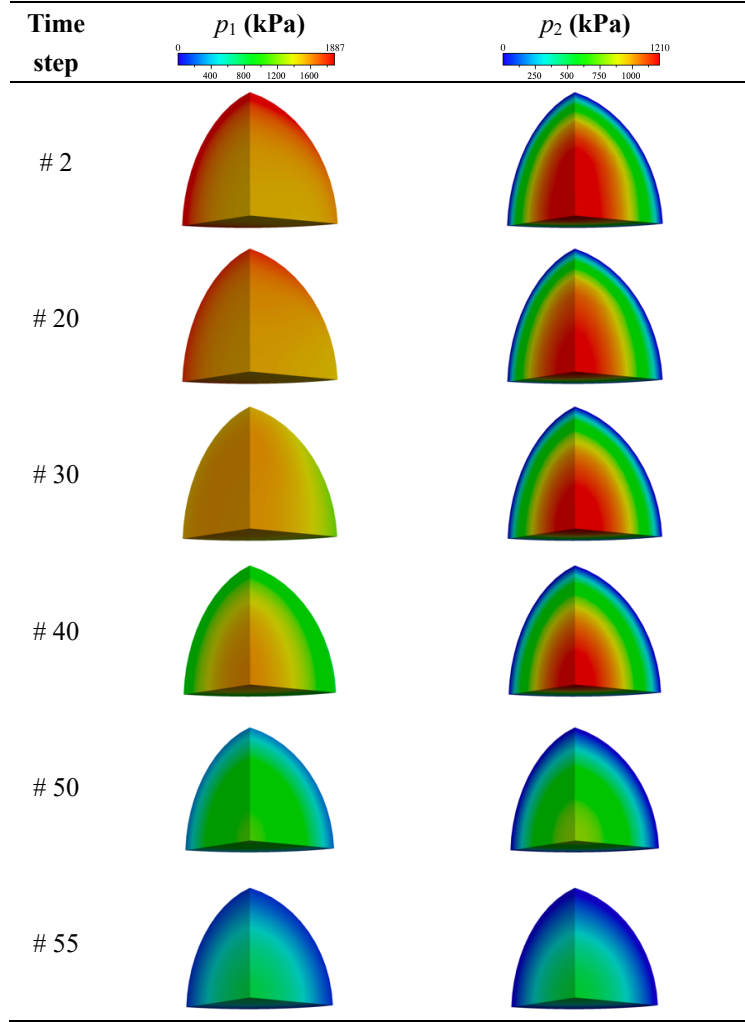


Figure 6: Evolutions of p_1 and p_2 in our saturated anisotropic poroelastic double porosity sphere.

From the last time step, since $p_1 \approx p_2 \approx 0$, we could obtain the largest amounts of compression in all three directions, they are $u_x^\infty = -0.071$ m, $u_y^\infty = -0.09792$ m and $u_z^\infty = -0.1551$ m. This anisotropic response is due to both the external load F and the mechanical properties. In other words, $|u_x^\infty| < |u_y^\infty|$ is because F is monotonically decreasing with $x \in [0, 1]$ m, and $|u_y^\infty| < |u_z^\infty|$ is because of $E_v < E_h$.

Another interesting finding is the non-monotone characteristic of p_2 at origin as shown in Fig. 7, which doesn't appear when \bar{k} is a constant or the magnitude of F is small. This difference is because when F is small, the magnitude of φ is also small, and from Eq. (28), a small φ_{\max} leads to $\bar{k} \equiv \bar{k}_{\min}$, so we would expect the same behaviors as $\bar{k}_{\max} = \bar{k}_{\min}$, i.e, constant \bar{k} . That's to say, the non-monotone characteristic of p_2 is related to a changing \bar{k} and a broad range of φ_{\max} compared with λ_{\max} .

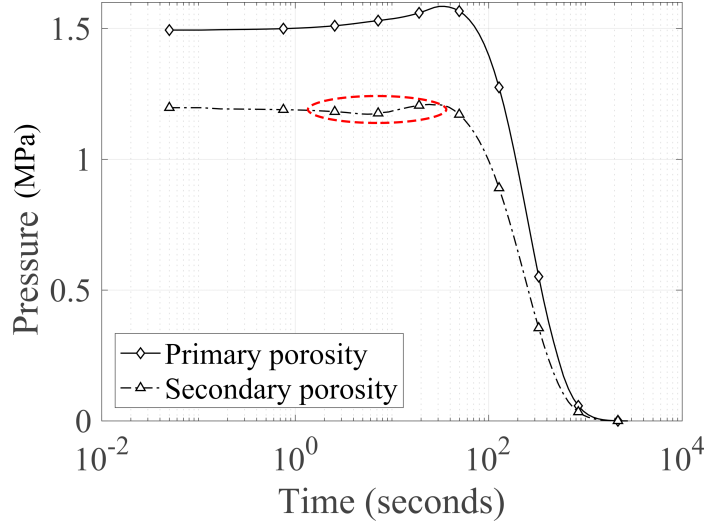


Figure 7: Time-variations of p_1 and p_2 at origin.

7. Conclusion

We have presented a comprehensive continuum framework for anisotropic and deformable porous materials exhibiting two dominant porosity scales with ultra-low matrix permeability. Through mathematical formulations, we have identified challenges in modeling $d\phi_1/dt$ and $d\phi_2/dt$. As a result, anisotropic constitutive equations for the porosities changes are proposed for the first time with coefficients A , α_1 , and α_2 . Scaling analysis is further implemented to provide mathematical evidence that we can ignore \bar{c} in the deformation equation. The finite element method is applied for the discretizations of fluid flow and solid deformation in our framework. Finally, the 3D numerical example demonstrates several facts:

1. A permeability tensor with a high anisotropy ratio may not skew the pressure distribution due to the combined effects of the principal directions of anisotropy and the drainage boundary.
2. The non-monotone characteristic of p_2 is related to a changing \bar{k} and a broad range of φ_{\max} compared with λ_{\max} .
3. The early time response of p_1 is dependent on the spatial distribution of external load F , while the late time responses of both scales tend to be the same.

Acknowledgments

This work was supported by the National Natural Science Foundation of China (Grant no. 51774199), the Shandong Provincial Natural Science Foundation, China (Grant no. ZR2015EL014), and the Qingdao Postdoctoral Applied Research project (Grant no. QDYY20190025). The first author acknowledges financial support provided by the John A. Blume Earthquake Engineering Center at Stanford University. We also deeply thank Prof. Ronaldo I. Borja (Stanford University) and Mr. Mark Ashworth (Heriot-Watt University) for comments and suggestions on the manuscript. In particular, Prof. Ronaldo I. Borja's expertise has helped to improve the manuscript substantially.

Appendix A. Supplement mathematical proof

Here we give a detailed proof of Eq. (13). By expanding the LHS, we get

$$\frac{\phi_1}{\rho_{1f}} \frac{d\rho_{1f}}{dt} + \frac{\nabla \cdot [\rho_{1f} \mathbf{q}_1]}{\rho_{1f}} = \frac{\phi_1}{\rho_{1f}} \frac{d\rho_{1f}}{dt} + \nabla \cdot \mathbf{q}_1 + \frac{\mathbf{q}_1 \cdot \nabla \rho_{1f}}{\rho_{1f}}. \quad (\text{A.1})$$

Next we replace \mathbf{q}_1 in the last term with its definition Eq. (9), we have

$$\frac{\phi_1}{\rho_{1f}} \frac{d\rho_{1f}}{dt} + \frac{\nabla \cdot [\rho_{1f} \mathbf{q}_1]}{\rho_{1f}} = \frac{\phi_1}{\rho_{1f}} \left[\frac{d\rho_{1f}}{dt} + (\hat{\mathbf{v}}_1 - \mathbf{v}_s) \cdot \nabla \rho_{1f} \right] + \nabla \cdot \mathbf{q}_1. \quad (\text{A.2})$$

Now if we subtract Eq. (4) from Eq. (5), we get

$$\frac{d^{1f}(\cdot)}{dt} = \frac{d(\cdot)}{dt} + \nabla(\cdot) \cdot (\hat{\mathbf{v}}_1 - \mathbf{v}_s). \quad (\text{A.3})$$

Replacing (\cdot) with ρ_{1f} and substituting Eq. (A.3) into Eq. (A.2) gives

$$\frac{\phi_1}{\rho_{1f}} \frac{d\rho_{1f}}{dt} + \frac{\nabla \cdot [\rho_{1f} \mathbf{q}_1]}{\rho_{1f}} = \frac{\phi_1}{\rho_{1f}} \frac{d^{1f} \rho_{1f}}{dt} + \nabla \cdot \mathbf{q}_1, \quad (\text{A.4})$$

and we finish the proof.

References

- [1] M. Ashworth, F. Doster, Foundations and their practical implications for the constitutive coefficients of poromechanical dual-continuum models, *Transport in Porous Media* (2019).
- [2] M. Bai, D. Elsworth, J. C. Roegiers, Multiporosity/multipermeability approach to the simulation of naturally fractured reservoirs, *Water Resources Research* 29 (1993) 1621–1633.
- [3] G. I. Barenblatt, Iu. P. Zheltov, I. N. Kochina, Basic concepts in the theory of seepage of homogeneous liquids in fissured rocks, *Journal of Applied Mathematics and Mechanics* 24 (1960) 852–864.
- [4] J. G. Berryman, H. F. Wang, The elastic coefficients of double porosity models for fluid transport in jointed rock, *Journal of Geophysical Research* 100 (1995) 611–627.
- [5] R. I. Borja, A. Koliji, On the effective stress in unsaturated porous continua with double porosity, *Journal of the Mechanics and Physics of Solids* 57 (2009) 1182–1193.
- [6] N. Castelletto, J. A. White, H. A. Tchelepi, Accuracy and convergence properties of the fixed-stress iterative solution of two-way coupled poromechanics, *International Journal for Numerical and Analytical Methods in Geomechanics* 39 (2015) 1593–1618.
- [7] H. Y. Chen, L. W. Teufel, Coupling fluid flow and geomechanics in dual porosity modeling of naturally fractured reservoirs, SPE Annual Technical Conference and Exhibition (1997).
- [8] A. H.-D. Cheng, Material coefficients of anisotropic poroelasticity, *International Journal of Rock Mechanics and Mining Sciences* 34 (1997) 199–205.
- [9] A. H.-D. Cheng, Poroelasticity, Springer (2016).
- [10] J. Choo, R. I. Borja, Stabilized mixed finite elements for deformable porous media with double porosity, *Computer Methods in Applied Mechanics and Engineering* 293 (2015) 131–154.
- [11] O. Coussy, Poromechanics, John Wiley and Sons (2004).
- [12] S. Dana, M. F. Wheeler, Convergence analysis of fixed stress split iterative scheme for anisotropic poroelasticity with tensor Biot parameter, *Computational Geosciences* 22 (2018) 1219–1230.
- [13] N. M. Dmitriyev, V. M. Maksimov, Non-linear laws of fluid flow through anisotropic porous media, *Journal of Applied Mathematics and Mechanics* 65 (2001) 935–940.
- [14] T. T. Garipov, M. Karimi-Fard, H. A. Tchelepi, Discrete fracture model for coupled flow and geomechanics, *Computational Geosciences* 20 (2016) 149–160.

[15] H. R. Ghafouri, R. W. Lewis, A finite element double porosity model for heterogeneous deformable porous media, *International Journal for Numerical and Analytical Methods in Geomechanics* 20 (1996) 831–844.

[16] R. Haggerty, S. M. Gorelick, Multiple-rate mass transfer for modeling diffusion and surface reactions in media with pore-scale heterogeneity, *Water Resources Research* 31 (1995) 2383–2400.

[17] S. Hansbo, Aspects of vertical drain design: Darcian or non-Darcian flow, *Géotechnique* 47 (1997) 983–992.

[18] F. Hao, L. S. Cheng, O. Hassan, J. Hou, C. Z. Liu, J. D. Feng, Threshold pressure gradient in ultra-low permeability reservoirs, *Petroleum Science and Technology* 26 (2008) 1024–1035.

[19] J. Jiang, J. Yang, Coupled fluid flow and geomechanics modeling of stress-sensitive production behavior in fractured shale gas reservoirs, *International Journal of Rock Mechanics and Mining Sciences* 101 (2018) 1–12.

[20] N. Khalili, A. P. S. Selvadurai, A fully coupled constitutive model for thermo-hydro-mechanical analysis in elastic media with double porosity, *Geophysical Research Letters* 30 (2003) 1–5.

[21] N. Khalili, S. Valliappan, C. F. Wan, Consolidation of fissured clays, *Géotechnique* 49 (1999) 75–89.

[22] J. Kim, Sequential methods for coupled geomechanics and multiphase flow, Ph.D. thesis, Stanford University (2010).

[23] J. Kim, E. L. Sonnenthal, J. Rutqvist, Formulation and sequential numerical algorithms of coupled fluid/heat flow and geomechanics for multiple porosity materials, *International Journal for Numerical Methods in Engineering* 92 (2012) 425–456.

[24] Q. Lei, W. Xiong, J. Yuan, S. Gao, Y. S. Wu, Behavior of flow through low-permeability reservoirs, SPE Europec/EAGE Annual Conference and Exhibition (2008).

[25] D. Li, W. Zha, S. Liu, L. Wang, D. Lu, Pressure transient analysis of low permeability reservoir with pseudo threshold pressure gradient, *Journal of Petroleum Science and Engineering* 147 (2016) 308–316.

[26] A. Mehrabian, Y. N. Abousleiman, Generalized Biot's theory and mandel's problem of multiple-porosity and multiple-permeability poroelasticity, *Journal of Geophysical Research: Solid Earth* 119 (2014) 2745–2763.

[27] H. F. Wang, Theory of linear poroelasticity with applications to geomechanics and hydrogeology, Princeton University Press (2000).

[28] X. Wang, J. J. Sheng, Effect of low-velocity non-Darcy flow on well production performance in shale and tight oil reservoirs, *Fuel* 190 (2017) 41–46.

[29] X. Wang, Z. Yang, Y. Sun, X. Liu, Experimental and theoretical investigation of nonlinear flow in low permeability reservoir, *Procedia Environmental Sciences* 11 (2011) 1392–1399.

[30] J. E. Warren, P. J. Root, The behavior of naturally fractured reservoirs, *SPE Journal* 3 (1963) 245–255.

[31] J. A. White, R. I. Borja, Stabilized low-order finite elements for coupled solid deformation/fluid diffusion and their application to fault zone transients, *Computer Methods in Applied Mechanics and Engineering* 197 (2008) 4353–4366.

[32] J. A. White, N. Castelletto, H. A. Tchelepi, Block-partitioned solvers for coupled poromechanics: A unified framework, *Computer Methods in Applied Mechanics and Engineering* 303 (2016) 55–74.

[33] R. K. Wilson, E. C. Aifantis, On the theory of consolidation with double porosity, *International Journal of Engineering Science* 20 (1982) 1009–1035.

[34] Y. Xiong, J. Yu, H. Sun, J. Yuan, Z. Huang, Y. S. Wu, A new non-Darcy flow model for low-velocity multiphase flow in tight reservoirs, *Transport in Porous Media* 117 (2017) 367–383.

[35] X. Yan, Z. Huang, J. Yao, Y. Li, D. Fan, H. Sun, K. Zhang, An efficient numerical hybrid model for multiphase flow in deformable fractured-shale reservoirs, *SPE Journal* 23 (2018) 1–26.

[36] X. Yan, Z. Huang, J. Yao, Y. Li, D. Fan, K. Zhang, An efficient hydro-mechanical model for coupled multi-porosity and discrete fracture porous media, *Computational Mechanics* 62 (2018) 943–962.

[37] B. Zeng, L. Cheng, C. Li, Low velocity non-linear flow in ultra-low permeability reservoir, *Journal of Petroleum Science and Engineering* 80 (2011) 1–6.

[38] Q. Zhang, Hydromechanical modeling of solid deformation and fluid flow in the transversely isotropic fissured rocks, *Computers and Geotechnics* 128 (2020).

[39] Q. Zhang, J. Choo, R. I. Borja, On the preferential flow patterns induced by transverse isotropy and non-Darcy flow in double porosity media, *Computer Methods in Applied Mechanics and Engineering* 353 (2019) 570–592.

[40] Q. Zhang, H. Zhu, Collaborative 3D geological modeling analysis based on multi-source data standard, *Engineering Geology* 246 (2018) 233–244.

[41] Y. Zhang, D. Zhang, Q. Fang, L. Xiong, L. Yu, M. Zhou, Analytical solutions of non-Darcy seepage of grouted subsea tunnels, *Tunneling and Underground Space Technology* 96 (2020).

[42] L. Zhao, H. Jiang, H. Wang, H. Yang, F. Sun, J. Li, Representation of a new physics-based non-Darcy equation for low-velocity flow in tight reservoirs, *Journal of Petroleum Science and Engineering* 184 (2020).